euspen's 25th International Conference & Exhibition, Zaragoza, ES, June 2025
www.euspen.eu

Improved Z-Map methodology through tool cutting edge discretization

Yasser Zekalmi [1*], José Antonio Albajez [1], María José Oliveros [1], Sergio Aguado [1]

[1] Design and Manufacturing Engineering Department, Universidad de Zaragoza, María Luna 3, Zaragoza, 50018, Spain

[1*] yzekalmi@unizar.es

Abstract

High quality components manufactured using 5-axis CNC milling in sectors such as aerospace, automotive or biomedical require an accurate surface finish. Traditional prediction methods are slow and complex, limiting their practical use. This contribution presents a novel, fast, and precise methodology, based on Z-Map method, to predict the 3D surface generated during milling operations. It precomputes the cutter's edge movement over an area of interest. Meanwhile, the intersection of the cutting edge and workpiece is parallelized. This approach enhances computational efficiency in surface prediction while maintaining accuracy. Moreover, the presented method is able to simulate different machining conditions and predict their effect on surface topography. This procedure enables manufacturers to optimize machining parameters more effectively, leading to better surface quality and reducing production times.

Topography, Computer numerical control (CNC), end milling, parallel

1. Introduction

High-precision machining is essential in industries like aerospace, automotive, and biomedical sectors, where surface quality impacts performance metrics such as fatigue resistance and dimensional accuracy. Predicting the micro-topography of machined surfaces in 5-axis CNC milling is particularly challenging due to the complex interplay between tool edge geometry, rotational dynamics, and machining parameters. While commercial CAM software can simulate macro-topography, accurately modeling micro-topography requires more advanced techniques.

These approaches are broadly classified into experimental and numerical methods [1]. Experimental techniques include the Taguchi method, space-time autoregressive models, and direct detection, [2]. Numerical methods, which excel in pre-machining simulations, include the N-buffer, Parallel Plane, Maximum Height, and Z-Map methods.

The N-buffer method calculates surface intersections of normal direction with the cutter edges and is adaptable for 3- and 5-axis milling, as shown by Chen et al. [3]. However, its computational cost is significant. The Parallel Plane method, developed by Arizmendi et al. [4], simplifies these calculations to intersections with parallel planes, but is limited to fixed-axis machining. The Maximum Height method models the cutter edges as curves and computes the maximum height cutted by a plane, efficiently calculates roughness for simple processes but lacks precision for complex surfaces, [5].

The Z-Map method, widely studied by Han et al. [6], offers simplicity and adaptability, but its accuracy depends on grid density. Xiao et al. [7] created an enhanced Z-Map algorithm based on sequential programming and treated the problem as an optimization, enhancing its applicability to advanced scenarios.

Among the various numerical methods proposed, the Z-map approach is widely used for its simplicity and ability to capture the topography accurately, [8]. However, its sequential processing and high computational cost for fine grid resolutions hinder its efficiency in handling large areas or complex tool paths. Recent enhancements, such as iterative and optimization-based methods, have improved accuracy but remain computationally intensive, [9].

This paper introduces a parallelized Z-map algorithm designed to overcome these limitations called PZMAP. By decoupling tool edge computation from workpiece intersection, PZMAP enables efficient parallel processing, significantly reducing computation times while maintaining high accuracy. This approach leverages modern hardware capabilities, offering a scalable and practical solution for predicting micro-topography in complex machining scenarios.

The paper is organized as follows: Section 2 describes the methodology and previous steps. Section 3 discussed the implementation of the parallelized algorithm. Section 4 outlines the results and validation through experiments. Finally, Section 5 discusses the conclusions of these findings and potential future research.

2. Methodology

The PZMAP methodology follows three main steps. It begins by importing machining data from CAM software. Next, it models the cutter's edge trajectory along the tool path (CL-data). Finally, it computes the intersections between the cutter's edges and the workpiece with a parallel algotithm to accurately predict the 3D topography.

2.1. Cutter's edge trajectory model

The cutter's edge trajectory is modeled using two primary coordinate systems: the fixed Workpiece Coordinate System (WCS) and the dynamic Tool Coordinate System (TCS). The WCS serves as the global reference, while the TCS moves with the tool, centered at the tool's center (TC) with its Z-axis aligned to the spindle. As shown in **Figure 1a**, the cutter's motion combines rotation and translation, generating the topography (purple

curve). **Figure 1b** highlights the cutter's geometry in TCS, the tool tip (TT), tool center (TC), and the cutter edges at consecutive time-steps (t and t+1).

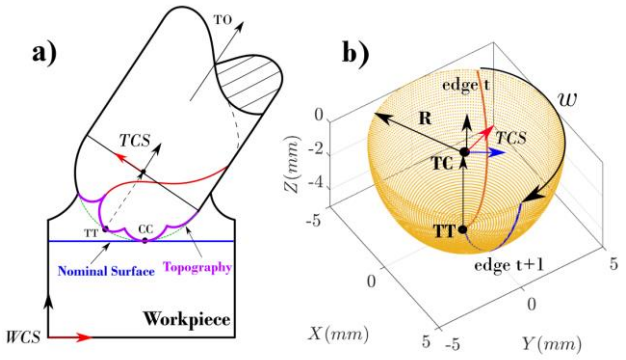

Figure 1. (a) Diagram of the topography generation. (b) Tool's diagram in TCS.

The tool studied in this paper is a ball end tool. The cutter edge is a curve with a helix angle γ and radius R. **Eq. 1** gives all cutter edge points, with θ from 0º to 90º, [10].

$$P_S = \begin{bmatrix} X \\ Y \\ Z \\ 1 \end{bmatrix} = \begin{bmatrix} R\sin\theta\cos\left(tan\gamma ln\left(cot\frac{\theta}{2}\right)\right) \\ R\sin\theta\sin\left(tan\gamma ln\left(cot\frac{\theta}{2}\right)\right) \\ -R\cos\theta \\ 1 \end{bmatrix} \quad (1)$$

In this paper, the area of interest (AOI) is filtered with the cutter contantact (CC) points of the tool, **Figure 2a**. Then, times for each CC point are computed with a constant feed speed (V_f) and the length of the tool path. With G01 movements, the cutter locations (CLs) are obtained using linear interpolation. **Figure 2b** shows the resulting movement of the swept cutter edge along the feed direction F and with a spindle speed ω.

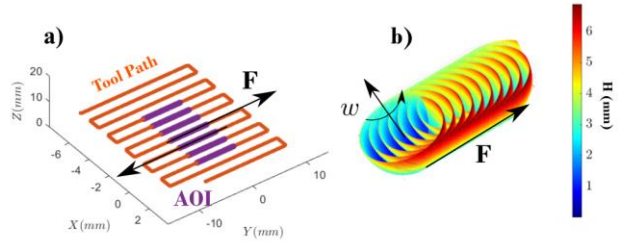

Figure 2. (a) Zig-Zag tool path. (b) Swept cutter's edge points along the tool path.

3. Intersection with the workpiece and PZMAP

The proposed PZMAP algorithm enhances computational efficiency by fully parallelizing the Z-map method. PZMAP improves performance by decoupling cutter edge computation from workpiece intersection. This decoupling enables two parallelizations. The first one is for cutter's edge computation, where each time step is sent to each core of the CPU. The second is in the intersection, where each subgrid is computed in each core, eliminating the need for sequential time-step loops common in traditional approaches. To optimize memory usage, PZMAP stores only cutter edge points below h_{max}, discarding the points that are not in contact with the workpiece and reducing storage requirements. Additionally, it employs single-precision coordinates to halve RAM usage without sacrificing accuracy, requiring approximately 10 GB for simulations. The cutter edge discretization is refined by computing angular limits (θ_{min} and θ_{max}) based on tool orientation and cutter contact points, further enhancing efficiency, **Figure 3.**

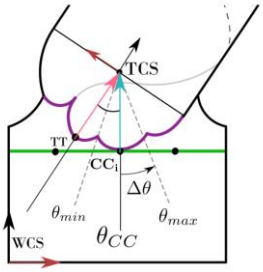

Figure 3. Cutter edge discretization based con the CC point.

Once all cutter edge points in the area of interest (AOI) are computed, the algorithm initiates parallel processing for the intersection with the workpiece. Diagonal points of a rectangle (d_1 and d_2) define the AOI, **Figure 4**. The workpiece is uniformly gridded with N_x and N_y points in the XY plane.

Each grid cell independently calculates the minimum height ($H_{i,j}$) from the stored cutter edge points above it. This avoids unnecessary neighbor checks, with each CPU core assigned to compute specific grid cells. The hardware has a built-in min function, which makes calculations much faster, especially when working with large sets of points.

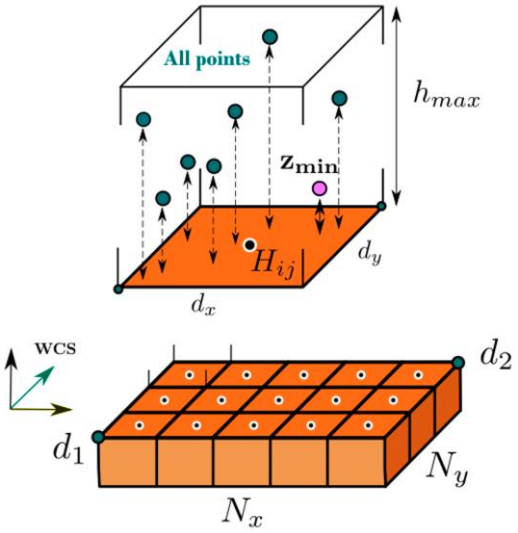

Figure 4. Scheme of the PZMAP intersection with the workpiece.

Figure 5 demonstrates the computational time reduction achieved through parallelization in the PZMAP algorithm across varying grid resolutions (N_{xy}) and core counts. At one core, the computational time reflects the classical Z-map method, highlighting its inefficiency, particularly at higher grid resolutions, where processing time exceeds 150 seconds for $N_{xy} = 150$. As the number of cores increases, the computational time decreases significantly, showcasing the efficiency of PZMAP's parallelization. Increasing from 1 to 8 cores reduces computational time from approximately 150 seconds to just 30 seconds, a fivefold improvement. Similar trends are observed across lower grid resolutions, though the absolute gains are smaller due to the reduced computational load.

This performance gain is due to the independent computation of each grid cell in PZMAP, which allows optimal utilization of

available CPU cores. The results demonstrate that PZMAP effectively scales with both grid size and hardware resources, making it far more efficient than the classical Z-map.

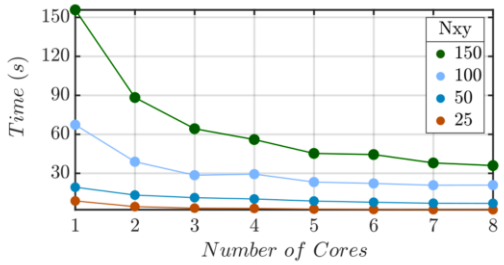

Figure 5. Computational times for different parallelization core numbers

4. Results and discussion

4.1. Experimental and simulation setup

Figure 6. shows the setup for the ball-end milling experiments. The machine used was a 3+2 axis HAAS VF3 with TRT160, and the axis movements were XYZAC. The ball-end milling tool was an IZAR HSS E/C08 with a 10 mm diameter, composed of steel with 8% Co, and featuring two cutter edges (N_{ed} = 2) with a helix start angle of 30º. In this study, we machined two areas in an Aluminium 7050 workpiece. The tool-path was generated in NX CAM with a zig-zag finishing strategy. The machining parameters are: spindle speed 3200 rpm, feed per tooth (f_z) of 0.04 mm/rev A1 and 0.24 mm/rev respectively. The maximum depth cut (h_{max}) is 0.5 mm and 10% of the diameter in stepover. The micro-topography was measured using an Alicona 3D optical microscope, with a resolution of 100 nm in Z and 2 µm in XY directions.

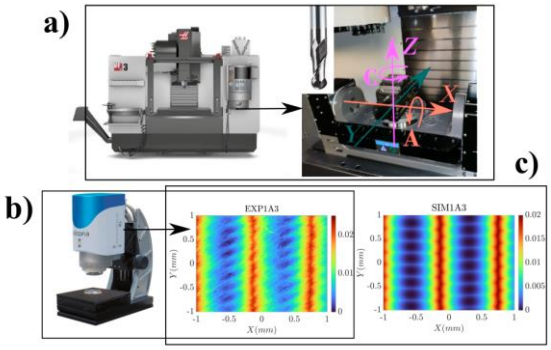

Figure 6. Diagram of the workflow. (a) Machining setup, (b) Measuring setup, and (c) Comparison of results.

The computer where all simulations are carried out is an Intel(R) Core(TM) i9-9980HK CPU at 2.6GHz, memory capacity 64 GB, Windows 10 system, software environment Matlab 2022a. The simulation parameters are set as follows: dt=1.25e-6s; $d\theta$=1e-3 rad; N_x and N_y = 100; and 8 cores for the parallel execution.

4.2. Experimental validation

The experimental and simulation results were analyzed to validate the proposed methodology, focusing on comparing the micro-topography produced under different feed rates. Two feed per tooth (f_z) values, 0.04 mm/rev and 0.24 mm/rev, were selected to highlight the surface profiles. **Figure 7** illustrates the results for f_z = 0.04 mm/rev. The experimental data (a) and simulation (b) exhibit similar periodic topography patterns, primarily driven by the trochoidal tool movement and the cutter edge engagement. The slice comparison at Y = 0 mm (c) shows good agreement between the experimental and simulated results.

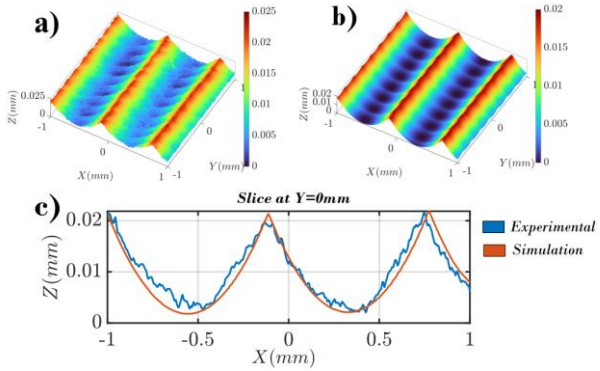

Figure 7. Results for f_z 0.04. (a) Experimental, (b) Simulation, and (c) Slice comparison at Y=0mm.

For f_z = 0.24 mm/rev, shown in **Figure 8.** , the surface topography becomes more prominent, with larger cusps along the feed direction, evident in both the experimental (a) and simulated (b) results. The slice at Y = 0 mm (c) confirms the consistency between the two datasets, with sharper peaks and deeper valleys compared to the lower feed rate. The simulation successfully reflects the effects of the increased feed rate on the surface micro-topography, demonstrating the robustness of the proposed methodology in capturing intricate details.

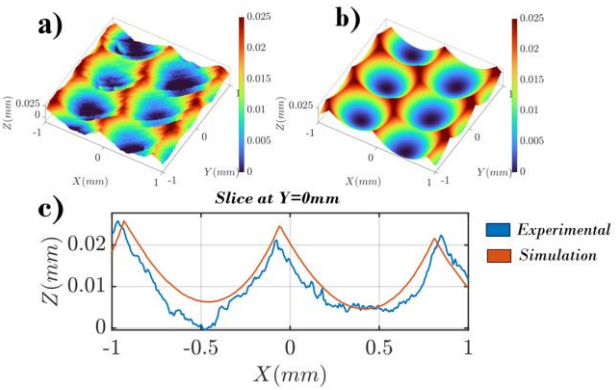

Figure 8. Results for f_z 0.24. (a) Experimental, (b) Simulation, and (c) Slice comparison at Y=0mm.

Overall, these results confirm that the simulation predicts the machined surface's micro-topography paterns under different feed rates, offering a reliable tool for machining process optimization. The maximum difference between the simulated and the experimental is around 5 μm.

4.3. Effect of f_z and N_{ed}

The surface micro-topography in ball-end milling is significantly influenced by the feed per tooth (f_z) and the number of cutter edges (N_{ed}). These factors dictate the interaction between the tool and workpiece, determining the peaks, valleys, and overall roughness of the machined surface.

In this section different scenarios where simulated. The metrics used to evaluate the 3D topography are the Pz (maximum height), **Eq. 2.**, and the Pa (average roughness) **Eq. 3**. Where Z is the height of a point in the topography and A is the area of a subgrid, [11].

$$\mathrm{Pz} = Z_{max} - Z_{min} \qquad (2)$$

$$Pa = \frac{1}{A}\int_A |Z(x,y)|dA \qquad (3)$$

The data in **Table 1** and **Table 2** illustrate how surface topography parameters respond to variations in feed per tooth (f_z) and the number of cutter edges. Pz (Table 1) generally increases as f_z grows, but adding more cutting edges helps moderate this rise. In other words, at higher feeds, using tools with more edges tends to reduce the maximum height variation of the surface. This indicates a more stable cutting action and potentially improved dimensional control. On the other hand, the Pa parameter (Table 2) remains comparatively steady and does not change as dramatically with variations in feed rate or cutter edges. While Pa increases slightly at higher feeds, the addition of more edges does not produce as pronounced an effect as observed in Pz. Essentially, the average roughness height tends to remain relatively uniform, even when feed or number of edges is adjusted.

Overall, the results suggest that increasing the number of cutter edges can significantly influence the peak-to-valley surface characteristics at higher feeds. This interplay can guide tool selection and feed optimization strategies to achieve the desired surface quality.

Table 1 Values of Pz (mm) for different f_z and number of cutter edges.

f_z (mm/rev)	Pz (μm), 2 edges	Pz (μm), 3 edges	Pz (μm), 4 edges
0.02	18.700	18.700	18.600
0.05	19.100	18.800	18.800
0.08	19.500	19.300	18.900
0.11	20.800	19.600	19.000
0.14	21.600	20.400	19.100
0.17	24.800	21.000	19.700
0.2	25.500	21.900	20.100
0.23	30.600	23.700	21.200

Table 2 Values of Pa (mm) for different f_z and number of cutter edges.

f_z (mm/rev)	Pa(μm), 2 edges	Pa (μm), 3 edges	Pa (μm), 4 edges
0.02	5.120	5.120	5.110
0.05	5.130	5.120	5.120
0.08	5.140	5.130	5.130
0.11	5.160	5.140	5.130
0.14	5.200	5.150	5.130
0.17	5.290	5.170	5.140
0.2	5.480	5.210	5.150
0.23	5.800	5.240	5.160

5. Conclusions

This work proposes an enhanced methodology for predicting three-dimensional surface topography in 5-axis CNC milling using ball-end cutters, improving speed over the classical Z-Map approach. This parallel algorithm PZMAP allows separating the cutter's edge computations from workpiece intersection. This approach achieves up to 10 times faster computation than the classical Z-Map method and accelerates The results of the experiments show very close resemblance to the predicted simulations validating the proposed methodology. This enhancement helps manufacturers to make informed decisions, enhancing product quality while reducing costs. Future research could scale these algorithm to larger freeform surfaces and complex toolpaths, while incorporating machine tool geometric inacurracies for more realistic modelling. Further exploration of advanced data structures and GPU acceleration could offer additional performance improvements.

References

[1] Y. Sun, Y. Liu, M. Zheng, J. Xu, and Q. Guo, "A review on theories/methods to obtain surface topography and analysis of corresponding affecting factors in the milling process," 2023. doi: 10.1007/s00170-023-11723-4.

[2] K. Zhao, R. Hockauf, Z. Liu, W. Zhao, X. Wang, and D. Wang, "Kinematic and stochastic surface topography of workpiece made of Al7075 in flank milling," *International Journal of Advanced Manufacturing Technology*, vol. 96, no. 5–8, 2018, doi: 10.1007/s00170-018-1709-3.

[3] C. H. Chiou, M. S. Hong, and K. F. Ehmann, "Simulation of machined surface topography in end-milling processes using a shear-plane-based cutting force model," in *Proceedings of the Institution of Mechanical Engineers, Part B: Journal of Engineering Manufacture*, 2004. doi: 10.1177/095440540421801211.

[4] M. Arizmendi, J. Fernández, A. Gil, and F. Veiga, "Model for the prediction of heterogeneity bands in the topography of surfaces machined by peripheral milling considering tool runout," *Int J Mach Tools Manuf*, vol. 50, no. 1, 2010, doi: 10.1016/j.ijmachtools.2009.09.007.

[5] A. Kukreja and S. S. Pande, "Estimation of scallop height in freeform surface CNC Machining," *International Journal of Advanced Manufacturing Technology*, vol. 104, no. 9–12, 2019, doi: 10.1007/s00170-019-04269-x.

[6] S. G. Han, J. Zhao, and X. F. Zhang, "Surface topography and roughness simulations for 5-axis ball-end milling," in *Advanced Materials Research*, 2009. doi: 10.4028/www.scientific.net/AMR.69-70.471.

[7] Y. Xiao, G. Ge, Z. Zeng, X. Feng, and Z. Du, "An improved Z-MAP method based on the SQP algorithm for fast surface topography simulation of ball-end milling," *International Journal of Advanced Manufacturing Technology*, vol. 128, no. 3–4, pp. 1863–1878, Sep. 2023, doi: 10.1007/s00170-023-11992-z.

[8] Z. Zhang, X. Lv, B. Qi, Y. Qi, M. Zhang, and Z. Tao, "Surface roughness prediction and roughness reliability evaluation of CNC milling based on surface topography simulation," *Eksploatacja i Niezawodnosc*, vol. 26, no. 2, 2024, doi: 10.17531/ein/183558.

[9] H. Gao *et al.*, "Simulation Study on Surface Topography and Roughness in Milling Process of Curved Die," *Integrated Ferroelectrics*, vol. 227, no. 1, 2022, doi: 10.1080/10584587.2022.2065570.

[10] W. Chen, W. Xie, D. Huo, and K. Yang, "A novel 3D surface generation model for micro milling based on homogeneous matrix transformation and dynamic regenerative effect," *Int J Mech Sci*, vol. 144, 2018, doi: 10.1016/j.ijmecsci.2018.05.050.

[11] ISO 21920-2:2021 Geometrical product specifications (GPS) — Surface texture: Profile — Part 2: Terms, definitions and surface texture parameters.